Available online at www.sciencedirect.com
ScienceDirect
Applied Surface Science 254 (2007) 760–764
applied surface science
www.elsevier.com/locate/apsusc

Magnetron sputter deposition of a 48-member cuprate superconductor library: $Bi_2Sr_2Y_xCa_{1-x}Cu_2O_{8+\delta}$ ($0.5 \leq x \leq 1$) linearly varying in steps of $\Delta x = 0.01$

R.J. Sanderson, K.C. Hewitt *

Dalhousie University, Department of Physics and Atmospheric Science, Halifax, Nova Scotia B3H 3J5, Canada

Received 31 January 2007; accepted 20 June 2007
Available online 13 July 2007

Abstract

Using magnetron sputtering, a spatial composition spread approach was applied successfully to obtain 48-member libraries of the $Bi_2Sr_2Y_xCa_{1-x}Cu_2O_{8+\delta}$ ($0.5 \leq x \leq 1$) cuprate superconducting system. The libraries of each system were deposited onto (1 0 0) single crystal MgO, mounted on a water cooled rotating table, using two targets: the antiferromagnetic insulator $Bi_2Sr_2YCu_2O_{8+\delta}$ ($P = 98$ W rf) and the hole doped superconductor $Bi_2Sr_2CaCu_2O_{8+\delta}$ ($P = 44$ W dc). A low chamber pressure of 0.81 mTorr argon was used to reduce scattering by the process gas. To minimize oxygen resputtering a substrate bias of −20 V was used, as well as a process gas free of oxygen. A rapid thermal processor was used to post-anneal the amorphous deposited films. A step annealing regime was used, with a ramp rate of 5 °C/s for heating and cooling, with a first plateau at 780 °C held for 200 s, and a second at 875 °C held for 480 s. X-ray diffraction reveals that the films develop crystalline order with the *c*-axis lattice parameter contracting linearly from 30.55 Å ($x = 0.5$) to 30.24 Å ($x = 1.0$) with increasing Y-content, consistent with bulk values. The crystallized films are polycrystalline, developing preferred orientation (*c*-axis parallel to the substrate) for thinner members of the library. There is a change of 0.01 in doping per library member which will enable further studies to densely map phase space.

PACS : 81.15.−z; 81.15.Cd; 74.78.−w; 74.78Bz; 74.72Hs; 68.55Nq

Keywords: Spatial composition spread; Combinatorial materials science; Cuprate superconductor; X-ray diffraction; Energy dispersive spectroscopy; Magnetron sputtering; Thin films; Bi-based cuprates; Phase composition

1. Introduction

It has been accepted for a long time that the temperature-hole concentration phase diagram holds the key to our understanding of the cuprate superconductors. Researchers have primarily sampled phase space discretely, using high quality single crystals, and have identified a number of important features such as the pseudogap [1]—a region of the phase diagram which is marked by the supression of low energy excitations below a temperature T^*. Understanding the doping dependence of this feature, especially near optimal doping ($p = 0.16$) is thought to hold the key to determining whether the pseudogap is a friend or foe of superconductivity [2]. That is, whether T^* merges with T_c, the superconducting onset temperature, or ends abruptly at optimal doping is thought to determine, respectively, whether the pseudogap phase is a precursor to, or competes with, superconductivity. Answering this question requires a dense map of phase space in order to trace the behaviour of T^* and T_c. Combinatorial materials science offers a method whereby such a dense map of phase space can be obtained.

Combinatorial materials science methods produce various compositions on a spatially addressable substrate. In particular, one may produce a continuous variation in composition across a substrate using physical vapor deposition techniques. This spatial composition spread approach is therefore of benefit when one wishes to map phase space densely. Although CMS methods have been used to show that particular superconducting phases can be prepared [3], to the author's knowledge the composition spread approach has not been used to map phase space of the cuprates and this report

* Corresponding author. Tel.: +1 902 494 2315; fax: +1 902 494 5191.
E-mail address: Kevin.Hewitt@dal.ca (K.C. Hewitt).
URL: http://www.physics.dal.ca/~hewitt/

0169-4332/$ – see front matter © 2007 Elsevier B.V. All rights reserved.
doi:10.1016/j.apsusc.2007.06.070

therefore represents the first step towards this goal. In this paper, the spatial composition spread approach is applied to the superconducting system $Bi_2Sr_2Y_xCa_{1-x}Cu_2O_{8+\delta}$, where x varies quasi-continuously between 0.5 and 1.

2. Experimental

The composition spread approach uses simultaneous, magnetron sputtering of two targets, e.g. A and B. Masks are placed over each target to produce a variation in the mass deposited onto a rotating substrate as described in more detail in reference [4]. When the mass, deposited onto the substrate, varies linearly for one target and is constant for the other, and the rotation speed is sufficient to intimately mix the atoms, by an appropriate choice of the powers applied to each target a film composition $A_{1-x}B_x$ ($0.5 \leq x \leq 1$) is produced. To produce $Bi_2Sr_2Y_xCa_{1-x}Cu_2O_{8+\delta}$ with $0.5 \leq x \leq 1$, one may therefore co-sputter two targets: A = $Bi_2Sr_2CaCu_2O_{8+\delta}$ (Bi-Ca-2212) and B = $Bi_2Sr_2YCu_2O_{8+\delta}$ (Bi-Y-2212).

2.1. Target preparation

Targets of nominal composition (slightly enriched with Ca and Sr) $Bi_{2.0}Sr_{2.05}Ca_{1.1}Cu_2O_{8+\delta}$ and $Bi_{2.0}Sr_{2.05}Y_{1.1}Cu_2O_{8+\delta}$ are made through the same three-stage solid-state reaction. Powders of Bi_2O_3 (99.975%, Alfa-Aesar), $SrCO_3$ (99.99%, Alfa-Aesar), CaO (99.95%, Alfa-Aesar) and CuO (99.7%, Alfa -Aesar) are mixed in the appropriate stoichiometric ratios and ground together for 2 h using an agate auto grinder. The mixture is placed in an Al_2O_3 crucible and reacted in air inside a Thermolyne 48000 box furnace. The first reaction, which calcinates the powders, is at 800 °C for 12 h (slow heat/slow cool at 4 °C/min). After the first reaction, the powder is ground for 2 h. The next two reactions are also in air and at a temperature of 875 °C. In between these two 875 °C reactions the powder is ground for 2 h. Once the target powders are synthesized, they are pressed into pucks and hardened before use. To accomplish this, the powder is ground manually with an agate mortar and pestle and sifted through a 70 μm sieve. Next, approximately 40 g of the sieved powder is pressed into a 5.08 cm (2 in.) diameter by 0.5 cm thick disc using a pressure of 13,000 psi. The disc is sintered for 30 h at 875 °C (Bi-Ca-2212) or 900 °C (Bi-Y-2212) to harden the target and reduce porosity.

2.2. Film deposition

The film deposition apparatus is a Corona Vacuum Coaters V-37 sputtering system equipped with 5 magnetrons configured in a side-sputtering arrangement (on-axis), where the substrate is directly across (5.5 cm) from the target. Fig. 1 depicts the deposition geometry, including the location of the substrates relative to the targets and schematics of the substrate and target masks. To power the magnetrons either an Advanced Energy MDX-1KDC supply or a combination of an Advanced Energy RFX-600 generator and RTX-600 tuner was chosen for the Bi-Ca-2212 (conductor) and Bi-Y-2212 (insulator) targets, respectively.

The film was deposited onto a water-cooled, rotating, table (43 cm diameter), upon which two sets of three 1 in. × 1 in. single crystal MgO (1 0 0) substrates (Superconductive Components Inc.) were placed radially to cover the 75 mm sputtering track. A slotted aluminum mask, consisting of fifty-six 0.5 mm slots separated by 1.52 mm, was placed over each set. The mask therefore produced a 48-member library. Thus, the difference in composition between each adjacent library member is $0.5/48 = 0.01$. In front of the Bi-Y-2212 target a mask was placed to produce a constant profile of mass deposited on the substrate while the Bi-Ca-2212 had a mask that produced a linear variation in mass deposited on the substrate.

The chamber was pumped down to a base pressure of 3.9×10^{-7} Torr, then an argon flow of 2 sccm was initiated to create a process gas pressure of 0.81 mTorr. It is important to note that oxygen was not added to the process gas as it leads to greater resputtering of the film. A bias of −20 V was applied to each mask using a carbon brush assembly (detailed elsewhere [5]).

The targets were co-sputtered while the substrate table rotated at constant rate of 15 rpm. The Bi-Ca-2212 target was powered by a dc supply operating at 44 W, while the Bi-Y-2212 target was powered by an rf supply operating at 98 W. These powers are chosen to produce equal sputtering rates, in order to deposit the desired range of compositions ($0.5 \leq x \leq 1$), where $x = [Y]/[Y + Ca]$.

2.3. Post-annealing

Post-annealing using a Rapid thermal Processor RTP-600S (Modular Process Technology Corp.) was performed on the amorphous as-deposited films in dry air. A step annealing regime was found to result in the best films. The regime starts with a ramp at 5 °C/s to 780 °C which is held for 200 s, followed by another ramp a 5 °C/s to 875 °C which is held for 480 s. The RTP is then cooled at 5 °C/s to room temperature.

2.4. Composition analysis

Composition of the films was determined using energy dispersive spectroscopy (EDS) measurements. Al foil strips were taped onto glass microscope slides and placed on the table. Following film deposition, the Al foil strips were removed from the microscope slides and affixed to an Al holder using double sided Cu tape. Post-annealed samples were measured on the MgO substrates by connecting the edges of the sample strips together with single sided Cu tape. The samples were analyzed for elemental composition using a JEOL JXA-8200 Superprobe energy dispersive spectrometer equipped with a Noran energy detector (0.133 keV energy resolution). A 7.0 kV electron beam with a 50 nA current is used to analyze a 10 μm spot of the film.

2.5. Structural analysis

For all deposited films, X-ray diffraction (XRD) spectra were collected using an Inel CPS-120 with a curved position

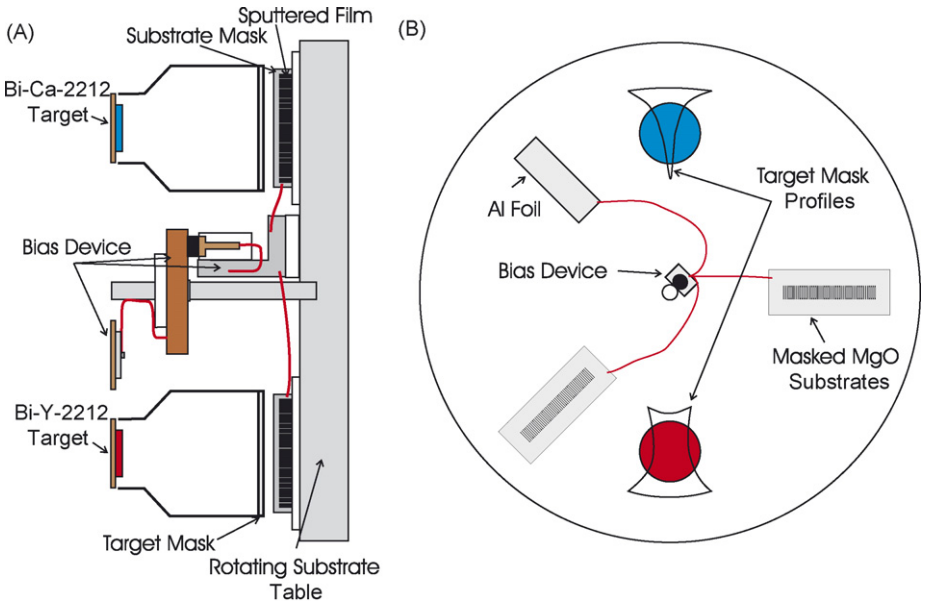

Fig. 1. (A) Side view of the on-axis sputtering geometry used for this experiment. (B) Table view of the deposition geometry, showing the substrate lay out as well as the target mask profiles.

sensitive detector. The Cu K α_1, α_2 X-ray beam is incident upon the sample at approximately 6° and the curved position sensitive detector collects all scattered X-rays from $2\theta = 4$–120°. Collection time for the XRD spectra is 1800 s per sample strip. The Inel has computer controlled translation stages to scan samples precisely and efficiently.

X-ray spectra were also collected using Siemens D500 and D5000 X-ray spectrometers. In both cases a single 1 in. × 1 in. piece of MgO was placed in the spectrometer with the set of strips parallel with the direction of the incoming beam and so during the measurement, the beam is incident on several strips. The D500 was used to collect conventional X-ray spectra ($\theta - 2\theta$ scans), while the D5000 was used to collect rocking curve spectra about the (0 0 1 6) peak of the Y-rich library members. The (0 0 1 6) peak is located at $2\theta = 48.08°$. For the rocking curve ω was chosen to be ±10° of the incident angle of 24.04°.

2.6. Thickness measurement

The film thickness was measured using a Veeco Dektak 8 M, by dragging a 12.5 μm stylus with a force of 24.4 μN over the film.

3. Results

An image of the post-annealed films are shown in Fig. 2. Included in the figure are axis showing the doping level (x) and the radial distance on the substrate table for each film strip. In the range 109–150 mm the film becomes thinner. Reasons for this will be discussed in subsequent sections.

The composition of the films before (on Al foil strips) and after (on MgO substrates) post-annealing treatment is shown in Fig. 3. These results clearly prove that post-annealing has no significant effect on the elemental ratios, given an error of 5% in the estimates.

The obvious question is whether the compositions in Fig. 3 reflect the Bi-2212 phase. While the Ca, Y content seems consistent with expectations, the Bi:Cu and Sr:Cu ratios seem systematically high, compared with the expected value (dashed line in Fig. 3). As a first step we determined the ratio of Bi:Sr, as shown in Fig. 4. It is clear from Fig. 4 that most of the values are in the range 0.7 to 1.15. It is known that Bi-2212 can be formed for a relatively large Bi:Sr range around 0.9–1.4 [6]. Therefore, one expects the structure to be consistent with Bi-2212 except perhaps in the range of radial distances 120–140 mm.

To understand this behaviour, the thickness of the library was measured at 10 points and the results are shown in Fig. 5. The library is 0.5–0.6 μm thick in the Y-rich range $x > 0.7$, changing gradually to 1.0–1.1 μm for Y-contents $x < 0.7$. The thickness does not change in a linear manner, which the linear plus constant profile should produce. However, as is evident in Fig. 3, there is some resputtering which would reduce the film thickness in the central region of the library, as observed in Fig. 5. The library image of Fig. 2 also shows effects of resputtering, as the film also looks to be thinner in the range 109–150 mm.

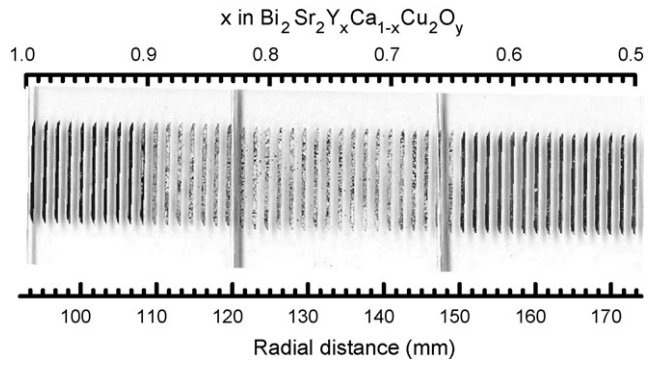

Fig. 2. Image of the 48-member library deposited on (1 0 0) MgO. There are actually 49 strips but one of these falls between two substrates near 148 mm and is not included in the Inel XRD analysis.

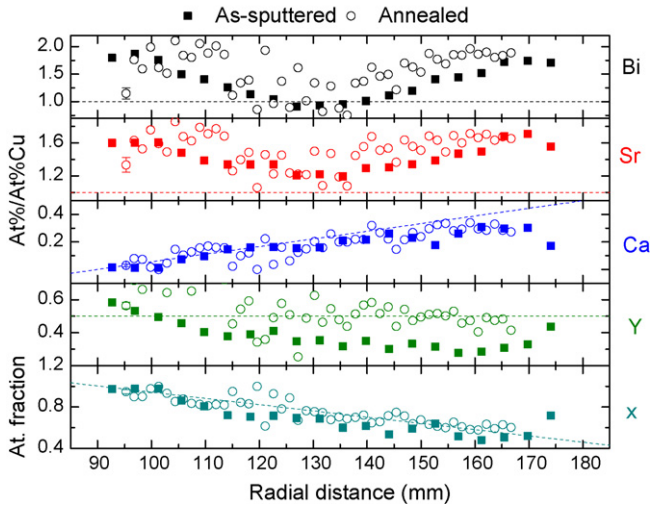

Fig. 3. Elemental composition (normalized to Cu) of the library (SPO099), as-deposited (filled squares) and after annealing (open circles). Dashed lines indicate target composition.

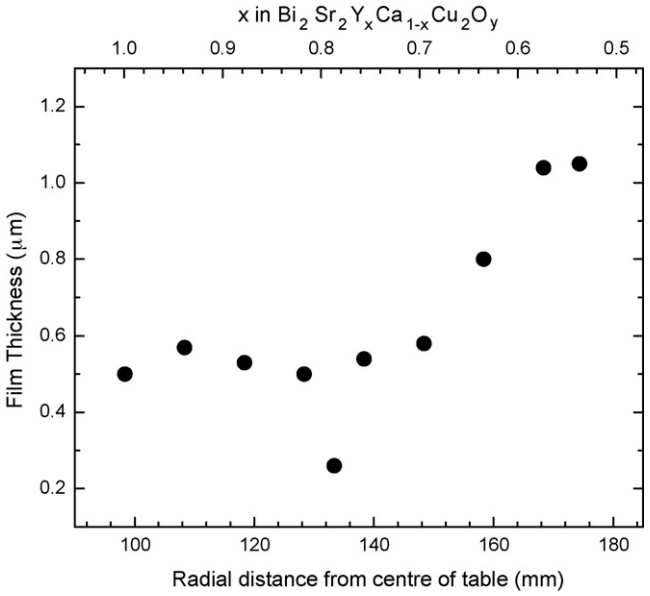

Fig. 5. The thickness at 10 points along the library.

To determine the structure and orientation of the film, X-ray diffraction was carried out for the entire library, using the Inel, and the results are shown as a 3D plot in Fig. 6. All but two of the peaks present can be indexed to the orthorhombic Bi-2212 structure, despite the range of Bi:Sr values seen in Fig. 4. It is surprising but fortuitous that Bi-2212 exists in the range 120–140 mm, given the Bi:Sr ratios. Reflections from (0 0 l) planes dominate the XRD patterns at the Y-rich end ($x \geq 0.7$). Given the Inel diffraction geometry (fixed incident X-ray and scattered X-rays collected over a large range of angles), one should not observe (0 0 l) reflections if the film is oriented with c-axis perpendicular to the film.

To determine the film characteristics more precisely, conventional $\theta - 2\theta$ scans were carried out using a Siemens D500 diffractometer. Fig. 7 shows X-rays spectra collected using the D500 for the entire library, divided into three sections corresponding to each substrate. The intensity of the X-ray spectra decreases dramatically from the Y-rich end (panel (A)) when compared to the Ca-rich end (panel (C)). This trend is likely due to incomplete crystallization of the Ca-rich films. The spectra of Fig. 7 shows the presence of several impurity peaks that were not readily evident from the Inel spectra of Fig 6. There are two identifiable Bi-2201 peaks as well as three Bi_2SrO_4 peaks. The increased presence of Bi-2201 in panel (B) is consistent with the decrease in Sr in the range of 110–150 mm shown in Fig. 3. Another feature in the D500 X-ray spectra (Fig. 7(A)) is the dominance of (0 0 l) reflections. This implies that the c-axis is preferentially oriented perpendicular to the

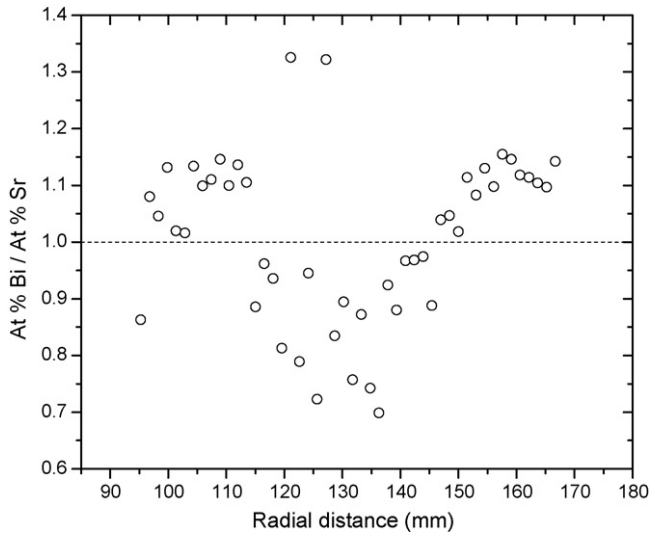

Fig. 4. The Bi:Sr elemental ratio of the post-annealed library as deduced from the open circles in the two upper panels of Fig. 3.

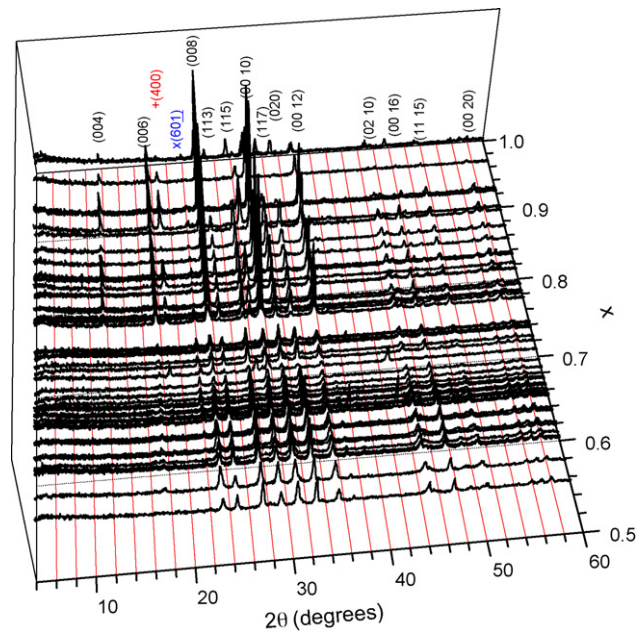

Fig. 6. Inel X-ray diffraction spectra of library (SP099), showing reflections consistent with Bi-2212. Also shown is a Bi-2201 (×) and Bi_2SrO_4 (+) peak.

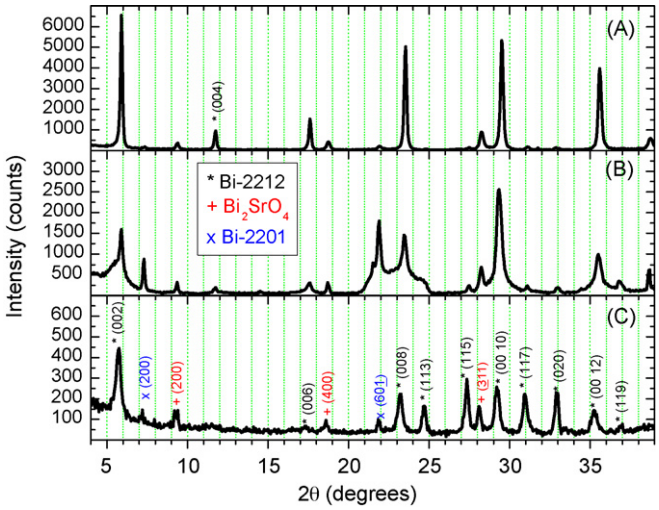

Fig. 7. Conventional $\theta - 2\theta$ scan X-ray diffraction spectra for each 1 in. × 1 in. MgO substrate. Panels (A–C) correspond to the Y-rich, center and Ca-rich substrates, respectively. Peak locations for Bi-2212, Bi-2201 and Bi_2SrO_4 are labeled.

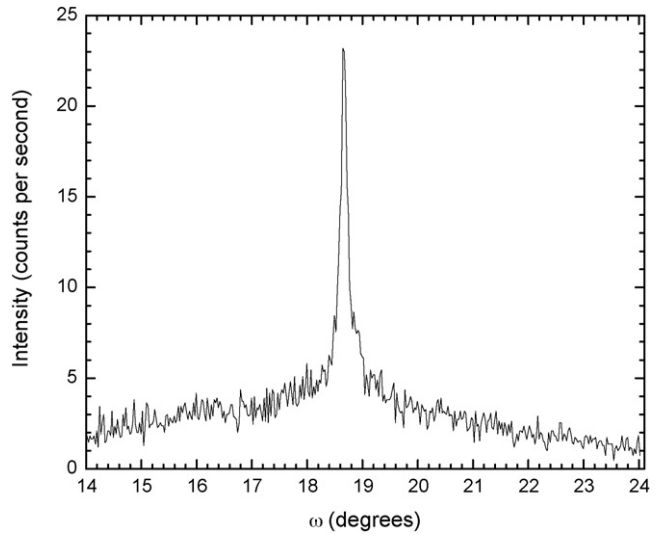

Fig. 8. X-ray rocking curve for the Bi-2212 (0 0 1 6) reflection from Y-rich library members ($x \geq 0.83$).

substrate. Pseuo-epitaxial growth is expected due to the reasonable lattice match with (1 0 0) MgO.

To reconcile the observations of Figs. 6(Y-rich end) and 7(A), a rocking curve measurement was completed to determine the *c*-axis mosaic spread of the film. The result is shown in Fig. 8. The sharp peak of the rocking curve clearly demonstrates that there is strong preferential orientation of the film. The rocking curve peak position of 23.4° is shifted by 0.6° from the expected 24.0°, which means that the *c*-axis is ever so slightly tilted (by 0.6°) relative to the MgO substrate. The rocking curve also sheds light on the Inel X-ray spectra of Fig. 6. The very broad and low intensity tails of the rocking curve is evidence that a small random orientated component is present within the sample. It is this latter component that is detected with the Inel measurement (Fig. 6).

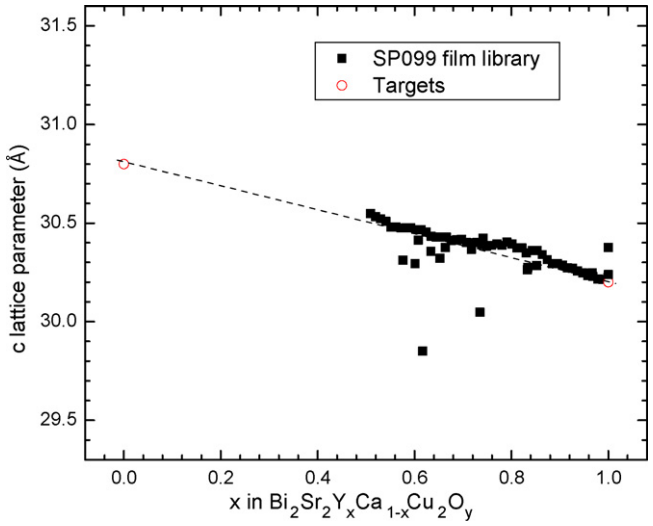

Fig. 9. The *c*-axis lattice parameter as a function of nominal composition for the library (filled squares) and targets (open circles).

Finally, the *c*-axis lattice parameter is determined in order to ascertain whether the changes are consistent with those of bulk Bi-2212 doped with Y. The results are plotted in Fig. 9. It reveals a trend that is clearly consistent with the change in magnitude of the parameter of the targets.

4. Conclusions

Structural and composition analysis has revealed that a spatial composition spread approach has been successfully applied to the cuprate superconductor system, $Bi_2Sr_2Y_xCa_{1-x}Cu_2O_{8+\delta}$ ($0.5 \leq x \leq 1$). A 48-member library is produced with the composition varying in a linear manner over the range $0.5 \leq x \leq 1$, corresponding to a change in Y-content of 0.01 per library member. The changes in the lattice parameter are consistent with those of bulk, and preferred orientation is observed for thinner members of the library. These films are now being used to densely map the electronic properties of phase space.

Acknowledgements

The financial support of the Natural Sciences and Engineering Research Council of Canada is gratefully acknowledged. KH would like to thank Ichiro Takeuchi for useful discussions.

References

[1] T. Timusk, B. Statt, Rep. Progr. Phys. 62 (1999) 61.
[2] M.R. Norman, D. Pines, C. Kallin, Adv. Phys. 54 (2005) 715.
[3] X.D. Xiang, X. Sun, G. Briceno, Y. Lou, K-A. Wang, H. Chang, W. Wallace-Freedman, S-W. Chen, P. Schultz, Science 268 (1995) 1738.
[4] J.R. Dahn, S. Trussler, T.D. Hatchard, A. Bonakdarpour, J.N. Meuller-Neuhaus, K.C. Hewitt, M. Fleischauer, Chem. Mater. 14 (2002) 3519.
[5] R.J. Sanderson, K.C. Hewitt, Physica C 425 (2005) 52.
[6] T.A. Vanderah, R.S. Roth, H.F. McMurdie (Eds.), Phase Diagrams for High-T Superconductors II, The American Ceramic Society, Westerville, OH, USA, 1997, pp. 211–214.